# Designing biphasic nanocellulose hydrogels to mimic the complex cartilage-bone interface

Sairash SAIRASH[1], Sirinee JIRAJESSADA[2], Pensuda SOMPUNGA[3], and Supansa YODMUANG[3,4,5,6,*]

[1] *Medical Science Program, Faculty of Medicine, Chulalongkorn University, Bangkok 10330, Thailand*

[2] *Biology Program, Faculty of Science, Buriram Rajabhat University, Muang, Buriram 31000, Thailand*

[3] *Research Affairs, Faculty of Medicine, Chulalongkorn University, Bangkok 10330, Thailand*

[4] *Center of Excellence in Biomaterial Engineering for Medical and Health, Chulalongkorn University, Pathumwan, Bangkok 10330, Thailand*

[5] *Clinical Excellence Center for Advanced Therapy Medicinal Products, King Chulalongkorn Memorial Hospital, Pathumwan, Bangkok 10330, Thailand*

[6] *Biomaterial Engineering for Medical and Health Research Unit, Chulalongkorn University, Bangkok 10330, Thailand*

**\*Corresponding author e-mail**: supansa.y@chula.ac.th

**Abstract**

Osteochondral lesions, which affect both the cartilage and the bone, present significant challenges in treatment due to the complex mechanical and biochemical properties of these tissues. A crucial consideration in developing tissue replacements for these lesions is the simultaneous regeneration of cartilage and calcified cartilage, which forms the transition zone to bone. Our current study aims to fabricate a bilayer polymeric hydrogel designed not only to support cartilage regeneration but also to serve as an interface between cartilage and bone. The bilayer hydrogel was created by combining oxidized bacterial nanocellulose, gelatin, and alginate in one layer, while the other layer consisted of the same three biopolymers and hydroxyapatite. The bacterial nanocellulose was effectively oxidized (20%) with sodium periodate and then mineralized with calcium and phosphorus (Ca/P ratio = 0.97), as confirmed by EDX analysis. Remarkably, both layers of the biphasic hydrogel demonstrated cytocompatibility with chondrocytes. Moreover, the addition of hydroxyapatite significantly improved the mechanical strength from 72 kPa (OBC/Gel/Alg) to 90 kPa (MOBC/Gel/Alg). This bilayer hydrogel holds promise for promoting bone-cartilage integration and has the potential to contribute to the healing of osteochondral defects, offering new possibilities in the field of orthopedic tissue engineering and regenerative medicine.

## 1. Introduction

Cartilage, devoid of a blood supply, lymphatic vessels, and nerve tissues, exhibits a limited capacity for self-repair. This inherent challenge renders cartilage susceptible to rapid deterioration following injury, contributing to joint damage, and making cartilage injuries the fourth most disabling disease globally [1,2]. Cartilage abnormalities often extend to the subchondral bone and some therapeutic techniques can even result in full thickness abnormalities. The limitations of previous surgcial techniques may be solved by tissue engineering (TE) of osteochondral composites, and it has been suggested as an alternate method of cartilage repair [1]. This underscores the imperative to develop innovative bio-scaffolds capable of providing distinct and tailored environments to guide the growth of both cartilage and subchondral bone tissues. Meeting the diverse biological and functional requirements of these two tissues within a single scaffold is the main point of attention [3]. Addressing this critical issue has prompted extensive research into the development of polymeric scaffolds for cartilage regeneration, a promising avenue explored by numerous researchers using both natural and synthetic materials.

The field of biomaterials offers four major classes that significantly contribute to osteochondral regeneration: natural polymers, synthetic polymers, inorganic biomaterials, and metallic biomaterials. Natural polymers, including cellulose, silk, polyester, polyamides, collagen, alginate, chitosan, and gelatin, emerge as vital components for regenerating cartilage zones [9-16]. Natural polymers are often combined with inorganic biomaterial, such as bioceramics, primarily calcium phosphates, to enhance mechanical stiffness, mirroring the biomimicry of the subchondral bone phase [4-8].

The realm of bone and cartilage regeneration has often been explored in isolation, with distinct methodologies developed for each tissue type. However, evolving perspectives acknowledge the intricate connection between cartilage and subchondral bone, prompts the consideration of integrated solutions, such as osteochondral implants [17]. This study aims to fabricate a bilayer polymeric hydrogel designed to serve as an interface between cartilage and bone. Positioned as a robust platform, the bilayer hydrogel holds promise for regenerating cartilage defects and supporting subchondral bone formation through the incorporation of inorganic hydroxyapatite. Cytotoxicity testing ensures the safety of a novel biolayer hydrogel, with future implications envisioning its role as scaffolds for cell attachment, specifically chondrocytes, presenting a comprehensive solution in osteochondral tissue engineering.

## 2. Experimental methods

### 2.1 Chemicals and reagents

Bacterial nanocellulose (BC) was kindly provided by Faculty of Engineering, Chulalongkorn University. Ethylene glycol ($C_2H_6O_2$, 324558), dibasic sodium phosphate ($Na_2HPO_4$, 94046), Sodium hydroxide (NaOH, S5881), Gelatin (300 bloom, type A), sodium alginate (W201502), sodium periodate ($NaIO_4$) (S1878), sodium chloride (NaCl) (S9888), dimethyl sulfoxide (DMSO) (D48418), Calcium Chloride ($CaCl_2$, C4901) were purchased from Sigma-Aldrich (St. Louis, MO, USA).

### 2.2. Polymers preparation, modification, and hydrogel formulation

#### 2.2.1 Preparation of bacterial nanocellulose (BC)

The BC pellicles were prepared by following a previously described procedure [18]. To start the biosynthesis process, we used a particularly chosen strain of A. xylinum (AGR60) and coconut water as culture media (sourced from the Burapha City Bang Wua Fresh Market in Chachoengsao, Thailand). This culture medium was enriched with defined concentrations of key components, including 5% (w/v) sucrose, 1% (v/v) acetic acid, and 0.50% (w/v) ammonium sulfate. The culture was kept at 30°C for 7 days. The BC pellicles were collected, rinsed with deionized water, and treated with 1% (w/v) sodium hydroxide solution. Then BC pellicles were rinsed with DI water until it reached pH 7, and stored at 4°C. The resulting BC pellicles were chopped into small pieces and blended for 15 min to get a fine slurry. BC slurry (30% w/v) suspension was mixed with DI water and homogenized at a speed of 15,000 rpm for 30 min and centrifuged at 4,000 rpm for 15 min to obtain purified BC.

#### 2.2.2 Oxidation of bacterial nanocellulose

Bacterial nanocellulose's oxidation was carried out in accordance with a previously described methodology [19]. Purified BC was soaked in KCl/HCl solution (250 mL of 0.2 mol·L$^{-1}$ KCl solution and 670 mL of 0.2 mol·L$^{-1}$ HCl solution mixed, pH 1) at room temperature. Next, the 17 g of this KCl/HCl treated BC were further mixed with 1% $NaIO_4$ specifically in a dark environment, at a high temperature of 90°C for 30 min without stirring [20]. An excess $NaIO_4$ was decomposed by the addition of ethylene glycol (12 mL) and incubated for 1 h at 25°C. Finally, the oxidized BC was washed several times to get rid of all residues and oxidizing agent.

#### 2.2.3 Mineralization of bacterial nanocellulose

Oxidized Bacterial Cellulose (OBC) along with their control native BC samples were deposited with calcium-deficient hydroxyapatite (CdHAP) by using a well-documented method [21-23]. The two-step immersion procedure is as follows: BC and OBC were initially soaked for 24 h in a solution containing 0.1 mol·L$^{-1}$ $CaCl_2$ and then immersed in a solution containing 0.06 mol·L$^{-1}$ $Na_2HPO_4$ for another 24 h while being constantly stirred at room temperature. The resulting groups mineralized oxidized bacterial nanocellulose (MOBC) and mineralized bacterial nanocellulose (MBC) were washed thoroughly with DI water.

#### 2.2.4 Preparation of hydrogel

The 0.5 g OBC or MOBC was mixed in 20 mL of DI water (2.5% w/v) and stirred well to get a homogenous suspension. Gelatin 2 g (10% w/v) was mixed in OBC and MOBC suspension by heat stirring for 24 h to obtain a gel-like solution. The powder of sodium alginate of 0.125 g (3.5% w/v) was dissolved completely in pre-heated OBC/Gel and MOBC/Gel solution at 50°C. Finally, the OBC/Gel/Alg solution and MOBC/Gel/Alg solution were poured into 12-well plate and kept at 4°C for 24 h for gelation. The resulting hydrogel discs were treated with $CaCl_2$ (2% w/v) for 1 h and washed with DI water to remove extra calcium and chloride ions.

### 2.3 Characterization

#### 2.3.1 Detection of dialdehyde content

The quantification of dialdehyde content within the lyophilized BC and OBC slurry samples was carried out using a previously described method [24,25]. First, the samples were treated with 20 mL of a 0.05 N NaOH solution for 15 min at 70°C. The solution was allowed to cool at room temperature and then treated with 10 ml of 0.1 N HCl solution. Finally, the dialdehyde group content of the scaffolds was determined by titrating with a 0.01 N NaOH solution until a neutral pH was reached. The calculation of dialdehyde group content was performed using the following formula [26]:

$$\text{mmol of dialdehyde groups} = \left( \frac{\text{volume of 0.01 M NaOH (mL)} \times \text{weight of scaffold (g)}}{100} \right)$$

The calculated dialdehyde group concentration was compared to the theoretical 100% degree of oxidation, which is 12.5 mmol·g$^{-1}$ to calculate the percentage of oxidation. FTIR Spectrometer Thermo Fisher (model: Nicolet IS5) was used to confirm oxidation of BC and OBC. The FTIR spectra were captured at a resolution of 4 cm$^{-1}$ in the wave number range of 4000 cm$^{-1}$ to 400 cm$^{-1}$.

#### 2.3.2 Microstructure of the mineralized bacterial nanocellulose

The microstructure of freeze-dried bacterial nanocellulose slurry and hydrogels were sputter-coated with Gold (Au) and examined using a scanning electron microscope (JSM-IT500HR, JEOL Group Companies, Japan). The imaging was carried out at an accelerating voltage of 10 kV. For the elemental analysis and mineral content determination of the bacterial nanocellulose samples, Energy dispersive X-ray spectroscopy (EDX) was conjugated with SEM. Additionally, the fiber diameter of fibers (n = 6) was measured by ImageJ software. (National Institutes of Health, NIH).

### 2.3.3 Swelling degree of hydrogel

Dry weigh and wet weight of the OBC/Gel/Alg and MOBC/Gel/Alg hydrogels were recorded. Swelling behavior of hydrogels was observed for 12 h until samples maintained their weight and reached to the equilibrium. Swelling degree was calculated using the formula [27].

$$\text{Swelling (\%)} = \frac{W_s - W_d}{W_d} \times 100$$

where Ws was weight swollen hydrogel and Wd was dry weight

### 2.3.4 Degradation behavior

As the hydrogel degradations in the body can occur through a combination of physical (dissolution), chemical (hydrolysis) and biological degradation (enzymatic) [28]. While lacking to replicate the complex and dynamic body in vivo environment due to its simple composition, PBS (Phosphate Buffer Saline) is still widely used as it mimics ionic strength and pH of the body fluids. In our study, the degradation behavior of OBC/Gel/Alg and MOBC/Gel/Alg hydrogels was investigated in 1xPBS at 37°C for 15 days. At biweekly, the samples were collected, rinsed with distilled water, and the wet weight were recorded [18,29]. The weight loss (%) of the hydrogels was calculated by using the wet weight at the initial time (Wi) and at any time (Wt), as the following equation:

$$\text{Weight loss (\%)} = \frac{W_i - W_t}{W_i} \times 100$$

### 2.3.5 Mechanical testing

Mechanical strength assessment of hydrogel constructs of 8 mm diameter and 3.5 mm height was carried out in 1xPBS by a Universal Testing machine (SHIMADZU), with 50% compression to original height or until sample breaks at a cross head speed of $0.5 \text{mm} \cdot \text{min}^{-1}$. Results were represented by the average value of 4 samples in each group.

### 2.4 Cytotoxicity assessment

In accordance with the ISO 109935:2009 standards for in vitro cytotoxicity assessment, hydrogel extracts (n = 4) were created. To prepare the hydrogel extract, OBC/Gel/Alg and MOBC/Gel/Alg hydrogels were incubated with DMEM media (serum-free) in a volume of $100 \text{ mg} \cdot \text{mL}^{-1}$, for 24 h in 5% $CO_2$ at 37°C. Parallelly, pig ear chondrocytes were seeded at a density of 2,000 cells per well of 96-well plate for 24 h in 100 μL of growth media (hDMEM medium containing 4% FBS, 1% antibiotic-antimycotic, 1% HEPES buffer). After that, the growth medium was replaced with 100 μL of OBC/Gel/Alg hydrogel extract or MOBC/Gel/Alg extract, positive control (10% DMSO in DMEM) for maximum cell death, or negative control (DMEM) for 24 h. Then cells were incubated with PrestoBlueTM solution in accordance with the manufacturer's instructions. The incubated medium was taken out and transferred to a 96-well plate. The fluorescence was measured at wavelengths of 560 nm for excitation and 590 nm for emission using a microplate reader (Varioskan Lux, Thermo Scientific, USA). All procedures performed involving stem cells

were reviewed and approved by the office of Institutional Review Board (IRB) of Faculty of Medicine, Chulalongkorn University.

### 2.5 LIVE/DEAD Staining

For the cell viability assessment, hydrogel constructs encapsulating adipose-derived stem cells (hADMSCs) were treated with Invitrogen LIVE/DEAD viability solution (2 mM calcien-AM and 4 mM ethidium homodimer-1 followed by manufacturer's instructions) for 30 min at 37°C in 5% $CO_2$. The assay solution was replaced with 1×PBS to wash out extra dye and samples were observed under a fluorescence microscope.

### 2.6 Statistical analysis

Quantitative data obtained was analyzed using Microsoft Excel and GraphPadPrism and presented as mean values with corresponding standard deviations, which were calculated from n = 4 samples within each group. In cases of analysis between groups, one-way analysis of variance (ANOVA) was performed followed by Bonferroni-corrected post-hoc tests for comparison between different groups. All analyses with a p-value of 0.05 or less were considered statistically significant.

## 3. Results and discussion

### 3.1 Fourier transform infrared (FTIR)

The chemical modification of BC via periodate oxidation was verified through FTIR analysis (Figure 1). The spectra of the samples focused on key vibrational bands, notably at 3341 $cm^{-1}$ (corresponding to O-H symmetrical stretching), 2894 $cm^{-1}$ (indicating C-H symmetrical stretching), 1426 $cm^{-1}$ and 1314 $cm^{-1}$ (representing the angular deformation of C-OH and C-$H_2$ coupled to OH), and 1160 $cm^{-1}$ (pertaining to the asymmetrical stretching of the β-glycosidic bond C-O-C) as observed in literature [30]. Sugiyama, Persson & Chanzy [31] previously demonstrated that signals in the proximity of 3240 $cm^{-1}$ are indicating of the existence of type Iα crystalline cellulose. It is
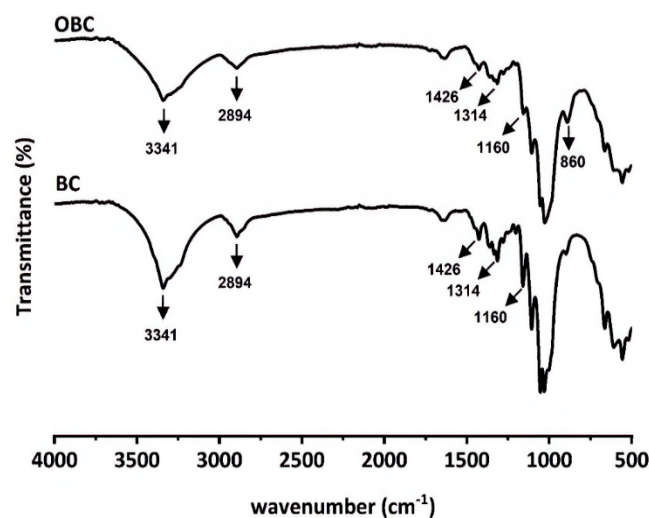


**Figure 1.** FTIR spectra of the oxidized bacterial nanocellulose (OBC) and native bacterial nanocellulose (BC).

known that the oxidation of BC by periodate involves the redox cleavage of vicinal (C2-C3) glycols, resulting in the formation of a substance known as 2,3-dialdehyde BC, which has aldehyde groups at the C2 and C3 locations of the glucopyranose unit [32]. The presence of the vibrational band around 860 cm$^{-1}$ confirms the successful oxidation of bacterial nanocellulose. This band corresponds to the hemiacetal and hydrate forms, as reported in similar studies [33]. The detection of this specific peak provides strong evidence for the modification of the nanocellulose structure. A number of structural configurations, such as free or hydrated aldehydes, hemialdols, and hemiacetals, can be produced via periodate oxidation [34]. The fact that this band is absent from the BC spectra provides a strong support for the idea that cellulose undergoes oxidation. The transformation of secondary alcohol groups into aldehyde groups is directly responsible for the decrease in vibrational band strength at 3341 cm$^{-1}$ in OBCs explaining the success of oxidation reaction as observed previously [20].

## 3.2   Degree of oxidation

The concentration of dialdehyde groups that sodium periodate oxidation introduced into the BC fibers were determined by acid-base titration was 2.5 mmol·g$^{-1}$, while native BC control groups did not showed any aldehyde content (Table 1), coinciding with the results of a previous case of OBC specifically using sodium periodate [20]. It is important to note that the 100% degree of oxidation converts to 12.5 mmol·g$^{-1}$ of dialdehyde groups inside the cellulose structure, which is comparable to each C2-C3 bond in the cellulose chain being converted into the 2,3-dialdehyde cellulose structure [26]. The outcomes indicate that OBC experienced modification during oxidation. Increasing the oxidant's concentration, extending the reaction time, or raising the reaction temperature can increase the degree of oxidation in these hydrogels [35]. The OBC may decrease mechanical strength and increase rate of disintegration. However, the OBC will allow mineral deposition.

## 3.3   Microstructure analysis of bacterial nanocellulose

The study examined morphological changes in bacterial nanocellulose (BC) fibers after oxidation and assessed the ability of both non-oxidized (BC) and oxidized (OBC) cellulose to promote the formation of bioactive nano-hydroxyapatite (nHA). Significant morphological differences were noted between the two groups, primarily due to the sodium periodate treatment in the OBC group. Despite these differences, both BC and OBC fibers demonstrated remarkable uniform dispersion (Figure 2, A and B respectively), consistent with previous findings [24,25,35]. The oxidized samples exhibited signs of fiber rupture, suggesting increased fragility likely linked to the loss of crystalline

structure resulting from extensive oxidation [36]. We found that the BC fiber diameter was slightly smaller than that of OBC fibers, ($52 \pm 3$ nm for BC and $58 \pm 3$ nm for OBC). For mineralized samples, the MBC ($52 \pm 4$ nm) and MOBC ($58 \pm 3$ nm) did not show significantly changes compared to their non-mineralized counterparts (Figure 2 C and D). It is important to note that the higher in fibril diameter may be attributed to a higher degree of oxidation, which is known to cause fibrils to aggregate more, resulting in larger average fiber diameters [21,24,25,37]. Further, it is remarkable to note that both OBC and MOBC showed almost same characteristics regarding the morphology and fiber diameter except the presence of nHA in MOBC confirming its mineralization. This observation aligns with the findings in our samples (Table 2)



Surface (Left) 20,000× , 1um      Cross-section (Right) 5000×, 5um
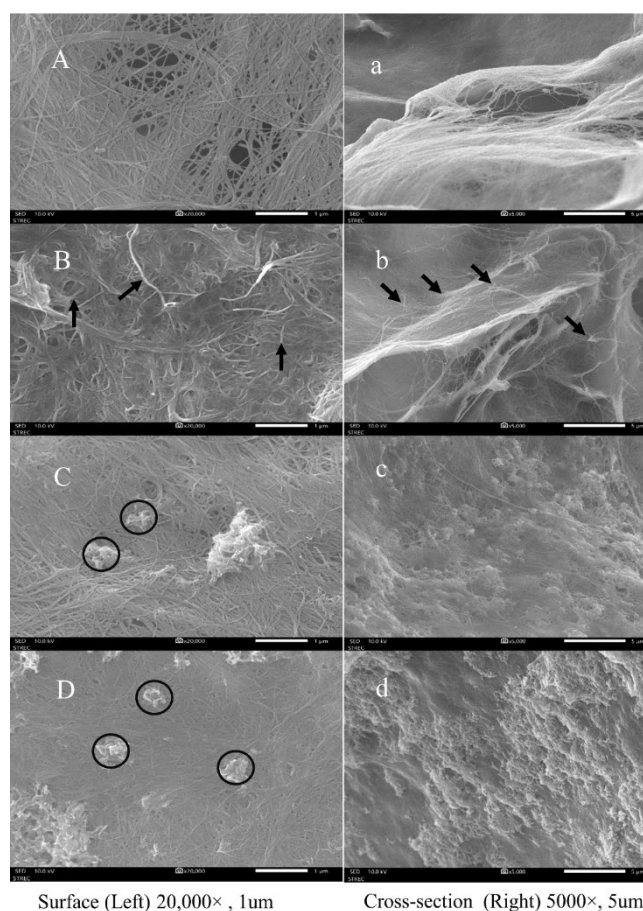
**Figure 2.** SEM micrographs of native bacterial nanocellulose (A and a), oxidized bacterial nanocellulose (B and b), mineralized bacterial nanocellulose (C and c), and mineralized oxidized bacterial nanocellulose (D and d). Arrows indicate fiber ruptures and aggregated fibrils in OBC. Circles indicate deposition of hydroxyapatite on mineralized bacterial nanocellulose groups (MBC and MOBC).

**Table 1.** Aldehyde content and % oxidation in bacterial nanocellulose samples.

| Samples | Dialdehyde content (mmol/g) | Oxidation degree (%) |
|---|---|---|
| Bacterial Cellulose (BC) | - | - |
| Oxidized Bacterial nanocellulose (OBC) | $2.5 \pm 0.023$ | $20 \pm 0.188$ |

**Table 2.** Average diameter of nanocellulose fibers**.**

| Samples | Fiber diameter (nm) |
|---|---|
| Bacterial nanocellulose (BC) | 52 ± 3 |
| Oxidized bacterial nanocellulose (OBC) | 58 ± 3 |
| Mineralized bacterial nanocellulose (MBC) | 52 ± 4 |
| Mineralized oxidized bacterial nanocellulose (MOBC) | 58 ± 3 |

**Table 3.** % Mass and Atomic mass of elements present in the samples BC, MBC, OBC and

| Elements hydrogel | | C | O | Na | P | Cl | Ca | K |
|---|---|---|---|---|---|---|---|---|
| BC | Mass % | 46.60±0.09 | 51.96±0.18 | 0.18±0.02 | | 0.68±0.02 | | 0.57±0.03 |
| | Atom % | 54.12±0.10 | 45.30±0.16 | 0.11±0.01 | | 0.27±0.01 | | 0.20±0.01 |
| MBC | Mass % | 29.38±0.09 | 44.57±0.17 | 6.27±0.06 | 9.75±0.07 | 0.46±0.02 | 9.58±0.09 | |
| | Atom % | 40.29±0.13 | 45.89±0.17 | 4.49±0.04 | 5.19±0.04 | 0.21±0.01 | 3.94±0.04 | |
| OBC | Mass % | 47.41±0.08 | 52.59±0.17 | | | | | |
| | Atom % | 54.57±0.09 | 45.43±0.15 | | | | | |
| MOBC | Mass % | 30.56±0.09 | 44.86±0.17 | 5.65±0.06 | 9.40±0.07 | 0.34±0.02 | 9.91±0.09 | |
| | Atom % | 41.47±0.13 | 45.69±0.17 | 4.00±0.04 | 4.94±0.04 | 0.15±0.01 | 3.74±0.04 | |

**Table 4.** Ca/P ratio in bacterial nanocellulose samples.

| Samples | Calcium (Ca) | Phosphate (P) | Ca/P |
|---|---|---|---|
| Bacterial nanocellulose (BC) | - | - | - |
| Oxidized bacterial nanocellulose (OBC) | - | - | - |
| Mineralized bacterial nanocellulose (MBC) | 9.58±0.09 | 9.75±0.07 | 0.982±0.012 |
| Mineralized oxidized bacterial nanocellulose (MOBC) | 9.19±0.09 | 9.40±0.07 | 0.978±0.012 |
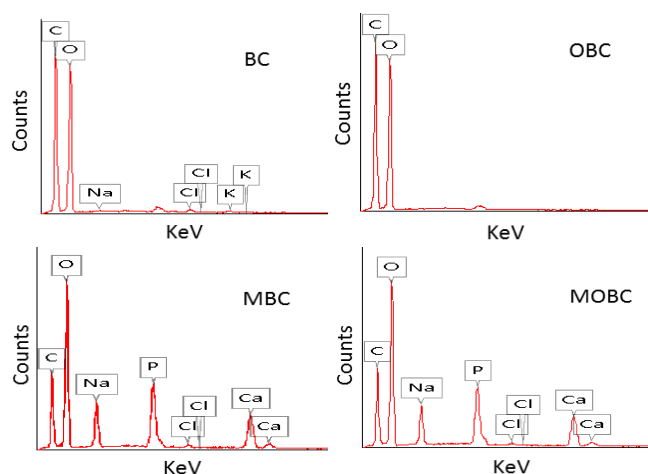


**Figure 3.** EDS spectra of elemental distribution in bacterial nanocellulose samples and calcium phosphate concentrations (Mass %) from EDS analysis of BC, OBC, MBC, and MOBC.

## 3.4 Energy dispersive X-ray analysis

Deposition of hydroxyapatite on mineralized bacterial nanocellulose groups (MBC and MOBC) was detected as small clusters within the nanocellulose fibers (Figure 2 C and D), which showed less hydroxyapatite crystals compared to previous study, where BC first underwent to phosphorylation and calcium deposition [36]. Corresponding with previous SEM results, leading to EDX analysis (Figure 3 and Table 3), the presence of calcium and phosphate in this study indicated apatite formation with Ca/P ratio of 0.98 and 0.97 for MBC and MOBC, respectively (Table 4). However, the Ca/P ratio was less than pure hydroxyapatite of 1.67 and previous report of 1.12 [37]. An increase

in mineralization cycles can increase calcium and phosphate ion precipitation from 1.13 to 1.6, resulting in considerable impact on the composition as well as the features of the deposited particles [38].

## 3.5 Microstructure analysis of the hydrogel

OBC/Gel/Alg and MOBC/Gel/Alg hydrogels exhibited porous structure throughout the cross-section (Figure 4) indicating a preferred scaffold morphology for cell culture as reported that a microporous scaffold helps in cell adhesion, cell migration, cell proliferation and differentiation along with facilitating the transportation of nutrients [27,39].
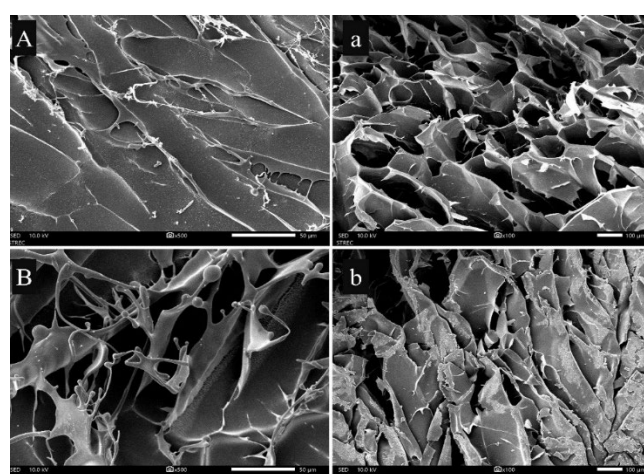


**Figure 4.** SEM images of lyophilized hydrogels. (A) OBC/Gel/Alg surface, (a) cross-section of OBC/Gel/Alg, (B) MOBC/Gel/Alg surface, (b) cross-section of MOBC/Gel/Al.

## 3.6 Swelling degree

The initial interaction between water and the polymeric network, known as swelling, is crucial in the realm of polymers to assess biomedical materials as it significantly effects transfer of nutrients, absorbption of tissue fluids and removal of wastes [40]. This process often precedes the disintegration of polymer chains and plays a vital role in cell adhesion and proliferation [43,44]. The articular cartilage ECM is primarily consist of water (68% to 85%), thus transporting nutrients to chondrocytes along with provinding lubrication [17].

In our study, we evaluated the swelling behavior of OBC/Gel/Alg and MOBC/Gel/Alg hydrogels (Figure 5). A significant disparity in water uptake capacity was observed which is indicative of their potential to mimic the natural ECM of cartilage. This water retention behavior aligns with a previous study, where a hydroxyapatite (HA) mineralized nanocellulose/gelatin scaffold for bone tissue engineering exhibited more swelling than a nanocellulose/gelatin scaffold without hydroxyapatite [45]. The high swelling observed in the MOBC/Gel/Alg hydrogel can be attributed to the presence of HA in MOBC, which imparts distinct hydrophilic characteristics that contribute to the increased swelling of HA-containing composite matrices [46,47]. In contrast, the OBC/Gel/Alg constructs exhibited lower hydrophilicity. This can be attributed to the inherently higher hydrophobic character of OBC, primarily due to the presence of aldehyde groups, which diminish hydrogen bond interactions with the hydroxyl groups on the bacterial nanocellulose (BC) [35].

If we compared the individual bacterial cellulose/Gelatin hybrid (that has reduced swelling due to high hydrophpobicity of OBC and supermolecular interactions [41]), and BC-Alginate (that poses a fluctuation in swelling behaviors due to the electrostatic repulsion and decresed osmotic pressure in ionically crosslinked hydrogel [42], we can conclude that the right combination of theses materials can lead to a significant improvement in the overall swelling behavior of OBC/Gel/Alg and MOBC/Gel/Alg hydrogel.

## 3.7 Degradation behavior

Bacterial nanocellulose (BC) samples exhibit low degradation rates in the body, although degradation can be accelerated through chemical modifications such as oxidation [43]. The biodegradation of dialdehyde nanocellulose (DAC) has garnered significant attention from researchers. A study by Singh et al. in 1982 revealed that DAC degrades into smaller molecules, including glycolic and 2,4-dihydroxy-butyric acid, when exposed to physiological pH levels [44]. In MOBC, a decrease in the degradability can be attributed to the isolated pairs in the aldehyde groups that coordinate the calcium ions, resulting in the formation of strong chemical bonds increasing its stability. Although hydroxyapatite (HA) in MOBC is considered stable under physiological conditions and even at mildly basic pH of 7.4 [45], some other studies confirmed that HA dissolves in vivo due to the response of an organism to a foreign component at an inflammation pH (pH 4-5) [46].

In our study, results indicate that degradation is more pronounced in the unmineralized hydrogel (OBC/Gel/Alg group) compared to the mineralized hydrogel (MOBC/Gel/Alg group) (Figure 5). This investigation highlights the importance of slow degradability in the presence of hydroxyapatite, which is beneficial for applications like guided bone regeneration. The modulation of the polymeric network and crosslinking offers significant potential for hydrogels in biomedical applications, especially those requiring controlled degradation. The unmineralized OBC/Gel/Alg hydrogel can be a favorable option for drug delivery systems requiring rapid degradation.

## 3.8 Mechanical assessment of hydrogel

While tested mechanically, both OBC/Gel/Alg and MOBC/Gel/Alg hydrogels exhibited compressive strength, with values in the range of $72 \pm 13$ kPa and $90 \pm 4$ kPa, respectively (Figure 6). These results suggest that the addition of mineral content to the MOBC/Gel/Alg hydrogel enhances its load-bearing capacity, making it a strong candidate for calcified cartilage and bone tissue engineering, as observed [47]. Consequently, in a biphasic hydrogel construct, the upper layer (OBC/Gel/Alg) is more favorable for cartilage tissue engineering, while the bottom layer (MOBC/Gel/Alg) is better suited for the development of calcified cartilage or bone tissue.

Mature native cartilage has a compressive strength of 14 MPa to 59 MPa [48], and human cancellous bone has a compressive strength of 1.5 MPa to 38 MPa [49]. We expected our biphasic hydrogel construct to have values falling between those of cartilage and bone, given its role as an interface between the two tissues. However, the cell-free biphasic hydrogel constructs in our study exhibited lower compressive strength than those of mature cartilage and bone. We anticipate that, with long-term tissue formation, the compressive strength of both OBC/Gel/Alg and MOBC/Gel/Alg hydrogels will increase.
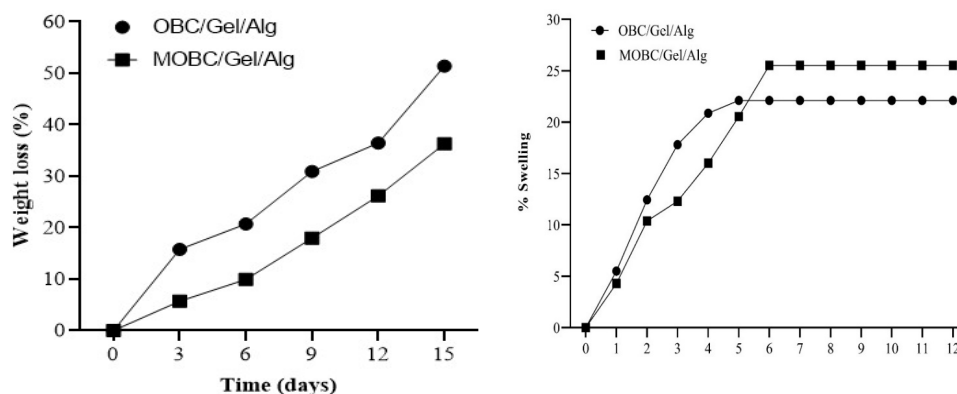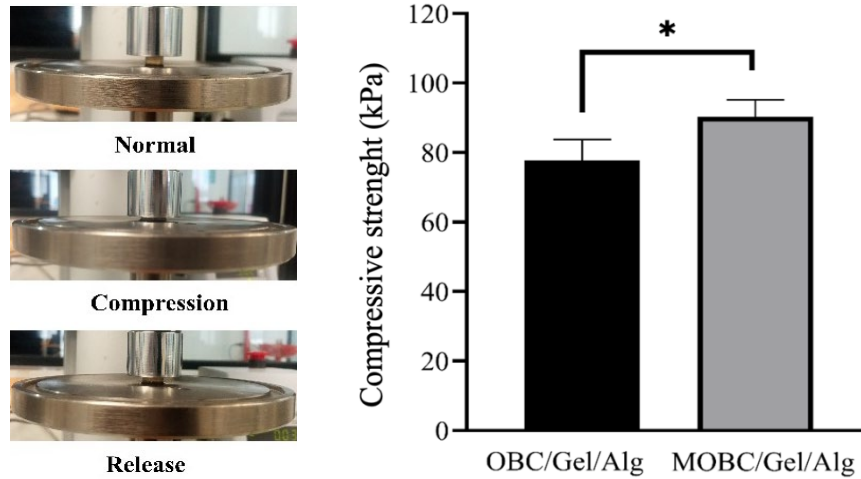


**Figure 5.** Swelling behavior and weight loss of polymeric hydrogels in 1xPBS.

**Figure 6.** Compressive Strength of Oxidized bacterial nanocellulose/Gelatin/ Alginate (OBC/Gel/Alg) and Mineralized Oxidized bacterial nanocellulose/ Gelatin/Alginate (MOBC/Gel/Alg) hydrogels, * P < 0.05.

## 3.9   Cytotoxicity of hydrogels

Excellent biocompatibility is a key attribute for hydrogels used as biomaterials in tissue engineering and regenerative medicine [50]. To assess the cytocompatibility and cell proliferation effects of the OBC/Gel/Alg and MOBC/Gel/Alg hydrogels, a cytotoxicity assay was performed using the PrestoBlue™ assay. The results indicated that neither hydrogel inhibited cell proliferation (Figure 7). The viability percentage of cultured chondrocytes in the hydrogel extracts showed a statistically significant difference ($P < 0.0001$) compared to the 10% DMSO positive control. The viability percentage of both hydrogel extracts remained above 70%, which is considered non-cytotoxic and biocompatible according to ISO 10993-5:2009 standards [51]. Furthermore, the addition of hydroxyapatite (HA) did not affect cell viability, showing the biocompatibility of the MOBC/Gel/Alg hydrogel, as observed in a previous study [45]. Based on these results, both types of hydrogel constructs proved to be non-toxic to cells and demonstrated excellent cell compatibility.
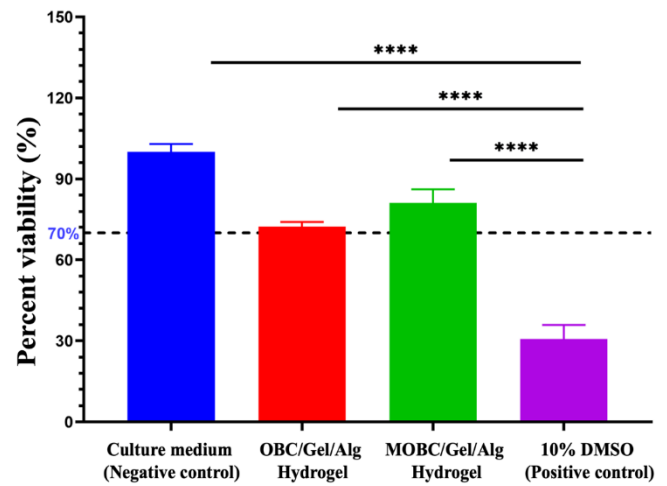


**Figure 7.** Cell viability. Chondrocytes were cultured in monolayer with culture medium, extract medium of OBC/Gel/Alg and MOBC/Gel/Alg hydrogels, or 10% DMSO. Data display as mean standard deviation (n=4); **** $P < 0.0001$.
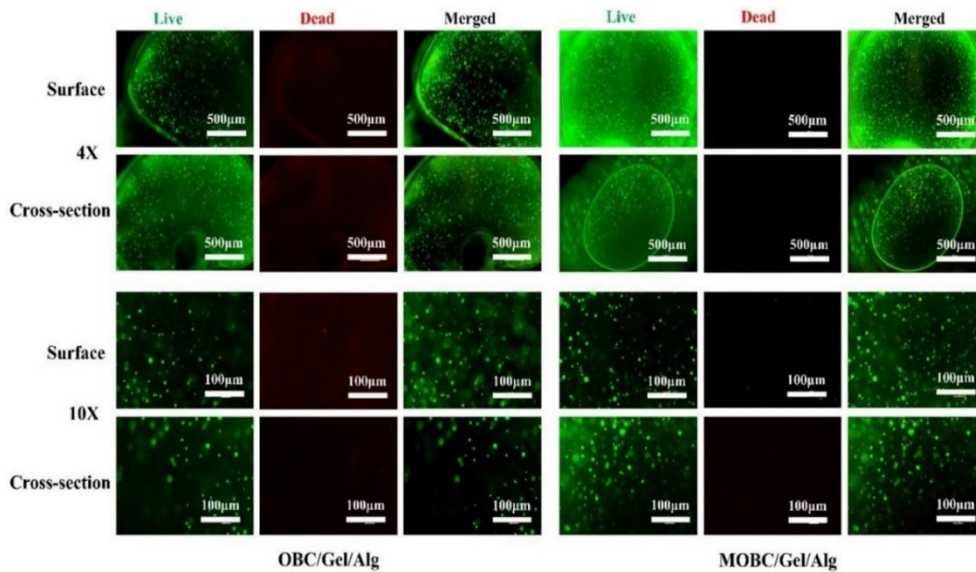


**Figure 8.** LIVE/DEAD staining of adipose-derived stem cells in OBC/Gel/Alg and MOBC/Gel/Alg hydrogels at day 3 post-encapsulation.

## 3.10 Cell distribution and viability assessment

For the tissue engineering applications, it is often desirable to achieve a dual characteristic in a scaffold to be porous for rapid nutrients and oxygen exchange along with providing a three-dimensional for encapsulated cells. This can be accomplished by fabricating porous, cell laden hydrogels [54].

In vitro cytocompatibility assessment of OBC/Gel/Alg and MOBC/Gel/Alg hydrogel were performed using the hADMSCs. For the surface and cross-sectional analysis of cell laden hydrogel constructs, LIVE/DEAD staining assay was performed on day 3 post-seeding (Figure 8). The hADMSCs showed a homogeneous distribution in both hydrogels (OBC/Gel/Alg and MOBC/Gel/Alg) as observed from surface and cross-sectional views under a fluorescence microscope, ensuring no cell clusters formed that could block nutrient and oxygen exchange.

Mineralized hydrogel (MOBC-Gel-Alg) in relation to oxidized sample (OBC/Gel/Alg hMSCs) showed more adhesion, spreading and viability with hMSCs. This may be attributed to the bioactive behavior of HA, increasing cytocompatibility [40,45].

## 4. Conclusions

Effective tissue replacements for osteochondral lesions must address the simultaneous regeneration of cartilage and the calcified cartilage that transitions to bone. In this study, a bilayer polymeric hydrogel was designed to support cartilage regeneration and serve as an interface between cartilage and bone. The bilayer hydrogel was fabricated with one layer combining oxidized bacterial nanocellulose, gelatin, and alginate, and a second layer incorporating the same biopolymers with added hydroxyapatite. Both layers of the biphasic hydrogel demonstrated excellent cytocompatibility with chondrocytes. The hydrogel's dual functionality underscores its potential as a pivotal component in osteochondral integration. Our innovative bilayer hydrogel introduces a promising approach in orthopedic tissue engineering and regenerative medicine, offering a potential solution for the treatment of osteochondral defects.

It is critical to further study cartilage and calcified cartilage development in this bilayer hydrogel by performing long-term culture of chondrogenic differentiation to determine if the transition zone formation actually occurs. We expect that our bilayer hydrogel will eliminate the need for additional adhesives at the calcified cartilage and bone interface, but this should be further investigated by conducting chondrogenic differentiation on top of bone plugs and measuring shear stress between the hydrogel and bone plug interface. Additionally, refining the fabrication process for up-scaled production of the bilayer hydrogel and assessing its in vivo response in animal studies are crucial steps toward its clinical applications.

## Credit authorship contribution statement

Sairash Sairash: Methodology, Visualization, Writing - Original Draft.
Sirinee Jirajessada: Visualization, Validate, Writing – Editing
Pensuda Sompunga: Data analysis, Validate

Supansa Yodmuang: Conceptualization, Investigation, Resources, Writing - Review & Editing

## Declaration of Competing Interest

The authors declare that they have no known competing financial interests or personal relationships that could have appeared to influence the work reported in this paper.

## Funding Information

## Acknowledgment

## References

[1]  J. F. Mano, and R. L. Reis, "Osteochondral defects: present situation and tissue engineering approaches," *Journal of Tissue Engineering and Regenerative Medicine,* vol. 1, no. 4, pp. 261-273, 2007.

[2]  N. Maffulli, U. G. Longo, N. Gougoulias, D. Caine, and V. Denaro, "Sport injuries: A review of outcomes," *British Medical Bulletin*, vol. 97, no. 1, pp. 47-80, 2011.

[3]  A. H. Gomoll, H. Madry, G. Knutsen, N. van Dijk, R. Seil, M. Brittberg, and E. Kon, "The subchondral bone in articular cartilage repair: current problems in the surgical management," *Knee Surgery Sports Traumatology, Arthroscopy,* vol. 18, no. 4, pp. 434-447, 2010.

[4]  B. Zhang, J. Huang, and R. J. Narayan, "Gradient scaffolds for osteochondral tissue engineering and regeneration," *Journal of Materials Chemistry B*, vol. 8, no. 36, pp. 8149-8170, 2020

[5]  B. Ye, B. Wu, Y. Su, T. Sun, and X. Guo, "Recent advances in the application of natural and synthetic polymer-based scaffolds in musculoskeletal regeneration," *Polymers*, vol. 14, no. 21, p. 4566, 2022.

[6]  G. Satchanska, S. Davidova, and P. D. Petrov, "Natural and synthetic polymers for biomedical and environmental applications," *Polymers*, vol. 16, no. 8, p. 1159, 2024.

[7]  I. Gorroñogoitia, U. Urtaza, A. Zubiarrain-Laserna, A. Alonso-Varona, and A. M. Zaldua, "A study of the printability of alginate-based bioinks by 3D bioprinting for articular cartilage tissue engineering," *Polymers*, vol. 14, no. 2, p. 354, 2022.

[8]  C. E. G. Garcia, B. Lardy, F. Bossard, F. A. S. Martínez, and M. Rinaudo, "Chitosan based biomaterials for cartilage tissue

engineering: Chondrocyte adhesion and proliferation," *Food Hydrocolloids for Health*, vol. 1, p. 100018, 2021.

[9]  Z. Montaseri, S. S. Abolmaali, A. M. Tamaddon, and F. Farvadi, "Composite silk fibroin hydrogel scaffolds for cartilage tissue regeneration," *Journal of Drug Delivery Science and Technology*, vol. 79, p. 104018, 2023.

[10]  M. A. Salati, J. Khazai, A. M. Tahmuri, A. Samadi, A. Taghizadeh, M. Taghizadeh, P. Zarrintaj, J. D. Ramsey, S. Habibzadeh, F. Seidi, M. R. Saeb, and M. Mozafari, "Agarose-based biomaterials: opportunities and challenges in cartilage tissue engineering," *Polymers (Basel)*, vol. 12, no. 5, p. 1150, 2020.

[11]  S. Barbon, M. Contran, E. Stocco, S. Todros, V. Macchi, R. De Caro, and A. Porzionato, "Enhanced biomechanical properties of polyvinyl alcohol-based hybrid scaffolds for cartilage tissue engineering," *Processes*, vol. 9, no. 5, p. 9050730, 2021.

[12]  A. M. Arnold, B. D. Holt, L. Daneshmandi, C. T. Laurencin, and S. A. Sydlik, "Phosphate graphene as an intrinsically osteoinductive scaffold for stem cell-driven bone regeneration," *Proceedings of the National Academy of Science of the United States of America*, vol. 116, no. 11, pp. 4855-4860, 2019.

[13]  M.-X. Yao, Y.-F. Zhang, W. Liu, H.-C. Wang, C. Ren, Y.-Q. Zhang, T.-L. Shi, and W. Chen, "Cartilage tissue healing and regeneration based on biocompatible materials: A systematic review and bibliometric analysis from 1993 to 2022," *Front Pharmacol,* vol. 14, pp. 1276849, 2024.

[14]  D. Khayatan, A. B. Oskouei, M. Alam, M. Mohammadikhah, A. Badkoobeh, M. Golkar, K. Abbasi, S. Karami, R. S. Soufdoost, and L. K. Hakim, A. Hussain, H. Tebyaniyan, and A. Heboyan, "Cross talk between cells and the current bioceramics in bone regeneration: A comprehensive review," *Cell Transplant,* vol. 33, p. 09636897241236030, 2024.

[15]  W. Wei, and H. Dai, "Articular cartilage and osteochondral tissue engineering techniques: Recent advances and challenges," *Bioactive Materials"* vol. 6, no. 12, pp. 4830-4855, 2021.

[16]  P. P. Phatchayawat, A. Khamkeaw, S. Yodmuang, and M. Phisalaphong, "3D bacterial cellulose-chitosan-alginate-gelatin hydrogel scaffold for cartilage tissue engineering," *Biochemical Engineering Journal*, vol. 184, p. 108476, 2022.

[17]  N. F. Vasconcelos, F. K. Andrade, L. d. A. P. Vieira, R. S. Vieira, J. M. Vaz, P. Chevallier, D. Mantovani, M. d. F. Borges, and M.F. Rosa, "Oxidized bacterial cellulose membrane as support for enzyme immobilization: properties and morphological features," *Cellulose,* vol. 27, no. 6, pp. 3055-3083, 2020.

[18]  E. Tsanaktsidou, O. Kammona, and C. N. Kiparissides, "Recent developments in hyaluronic acid-based hydrogels for cartilage tissue engineering applications," *Polymers,* vol. 14, no. 4, p. 839, 2022.

[19]  Y. Wan, L. Hong, S. Jia, Y. Huang, Y. Zhu, Y. Wang, H. J. Jiang, "Synthesis and characterization of hydroxyapatite–bacterial cellulose nanocomposites," *Composites Sciencd and Technology,* vol. 66, no. 11-12, pp. 1825-1832, 2006.

[20]  P. M. Favi, S. P. Ospina, M. Kachole, M. Gao, L. Atehortua, and T. J. Webster, "Preparation and characterization of bio-degradable nano hydroxyapatite–bacterial cellulose composites with well-defined honeycomb pore arrays for bone tissue engineering applications," *Cellulose*, vol. 23, pp. 1263-1282, 2016.

[21]  K. Pommerening, H. Rein, D. Bertram, and R. Müller, "Estimation of dialdehyde groups in 2, 3-dialdehyde bead-cellulose," *Carbohydrate Research*, vol. 233, pp. 219-223, 1992.

[22]  P. Roychowdhury, and V.Kumar, "Fabrication and evaluation of porous 2,3-dialdehydecellulose membrane as a potential biodegradable tissue-engineering scaffold," *Journal of biomedical Material Research: Part A*, vol. 76, no. 2, pp. 300-309, 2006.

[23]  Z. Li, X. Chen, C. Bao, C. Liu, C. Liu, D. Li, H. Yan, and Q. Lin, "Fabrication and evaluation of alginate/bacterial cellulose nanocrystals–chitosan–gelatin composite scaffolds," *Molecules*, vol. 26, no. 16, p. 5003, 2021.

[24]  M. N. Egorikhina, I. I. Bronnikova, Y. P. Rubtsova, I. N. Charykova, M. L. Bugrova, D. D. Linkova, and D. Y. Aleynik, "Aspects of in vitro biodegradation of hybrid fibrin–collagen scaffolds," *Polymers*, vol. 13, no. 20, p. 13203470, 2021.

[25]  H. Yan, D. Huang, X. Chen, H. Liu, Y. Feng, Z. Zhao, Z. Dai, X. Zhang, and Q. Lin, "A novel and homogeneous scaffold material: Preparation and evaluation of alginate/bacterial cellulose nanocrystals/collagen composite hydrogel for tissue engineering," *Polymer Bulletin*, vol. 75, no. 7, pp. 1-16, 2018.

[26]  Y. Yu, W. Guo, J. Qu, S. Wang, X. Wang, Y. He, Y. Yang, Q. He, X. Liu, "Preparation and characterization of dialdehyde cellulose nanocrystals from the waste nutshell," *Environment, Development and Sustainability*, vol. 1, pp. 1-17, 2023.

[27]  J. Sugiyama, J. Persson, and H. Chanzy, "Combined infrared and electron diffraction study of the polymorphism of native celluloses," *Macromolecules*, vol. 24, no. 9, pp. 2461-2466, 1991.

[28]  J. Wu, Y. Zheng, Z. Yang, Q. Lin, K. Qiao, X. Chen, and Y. Peng, "Influence of dialdehyde bacterial cellulose with the nonlinear elasticity and topology structure of ECM on cell adhesion and proliferation," *RSC Advances*, vol. 4, no. 8, pp. 3998-4009, 2014.

[29]  U. J. Kim, S. Kuga, M. Wada, T. Okano, and T. Kondo, "Periodate oxidation of crystalline cellulose," *Biomacromolecules*, vol. 1, no. 3, pp. 488-492, 2000.

[30]  Q. Fan, D. Lewis, and K. N. Tapley, "Characterization of cellulose aldehyde using Fourier transform infrared spectro-scopy," *Journal of Applied Polymer Science*, vol. 82, no. 5, pp. 1195-1202, 2001.

[31]  L. M. de Vasconcelos, N. Vasconcelos, D. Lomonaco, M. de Freitas Rosa, E. Rodriguez-castellon, F. K. Andrade, and R. S. Vieira, "Microwave-assisted periodate oxidation as a rapid and efficient alternative to oxidize bacterial cellulose wet membrane," *Polymer Bulletin*, vol. 80, pp. 11861-11881, 2023.

[32]  E. Höglund, "Production of dialdehyde cellulose and periodate regeneration: Towards feasible oxidation processes," *Chemical Sciences*, p. 36, 2015

[33]  J. Li, Y. Wan, L. Li, H. Liang, and J. Wang, "Preparation and characterization of 2,3-dialdehyde bacterial cellulose for potential biodegradable tissue engineering scaffolds,"

*Materials Science and Engineering: C,* vol. 29, no. 5, pp. 1635-1642, 2009.

[34] Y. Wan, Y. Huang, C. D. Yuan, S. Raman, Y. Zhu, H. J. Jiang, F. He, and C. Gao, "Biomimetic synthesis of hydroxyapatite/ bacterial cellulose nanocomposites for biomedical applications," *Materials Science and Engineering: C,* vol. 27, no. 4, pp. 855-864, 2007.

[35] F. Nurlidar, E. Budianto, D. Darwis, and Sugiarto, "Hydroxyapatite deposition on modified bacterial cellulose matrix," *Macromolecular Symposia*"vol. 353, no. 1, pp. 128-132, 2015.

[36] A. Cañas-Gutiérrez, L. Toro, C. Fornaguera, S. Borrós, M. Osorio, C. Castro-Herazo, and D. Arboleda-Toro, "Biomineralization in three-dimensional scaffolds based on bacterial nanocellulose for bone tissue engineering: Feature characterization and stem cell differentiation," *Polymers*, vol. 15, no. 9, p. 15092012, 2023.

[37] X. Song, C. Zhu, D. Fan, Y. Mi, X. Li, R. Z. Fu, Z. Duan, Y. Wang, and R. R. Feng, "A novel human-like collagen hydrogel scaffold with porous structure and sponge-like properties," *Polymer (Basel),* vol. 9, no. 12, p. 638, 2017.

[38] Z. Li, H. Liu, Y. Liao, H. Wang, X. Sun, X. Chen, H. Yan, and Q. Lin, "Design and properties of alginate/gelatin/ cellulose nano-crystals interpenetrating polymer network composite hydrogels based on in situ cross-linking," *European Polymer Journal*, vol. 201, pp. 112556, 2023.

[39] F. Farshi Azhar, A. Olad, and R. Salehi, "Fabrication and characterization of chitosan-gelatin/nanohydroxyapatite-polyaniline composite with potential application in tissue engineering scaffolds," *Designed Monomers and Polymers*, vol. 17, no. 7, pp. 654-667, 2014.

[40] E. P. C. G. Luz, P. H. S. Chaves, L. d. A. P. Vieira, S. F. Ribeiro, M. de Fátima Borges, F. K. Andrade, C. R. Muniz, A. Infantes-Molina, E. Rodríguez-Castellón, M. de Freitas Rosa, and R. S. Vieira, "In vitro degradability and bioactivity of oxidized bacterial cellulose-hydroxyapatite composites," *Carbohydrate Polymers*, vol. 237, p. 116174, 2020.

[41] W. Habraken, P. Habibovic, M. Epple, and M. Bohner, "Calcium phosphates in biomedical applications: materials for the future?," *Materials Todey,* vol. 19, no. 2, pp. 69-87, 2016.

[42] H. Wang, B. Hu, H. Li, G. Feng, S. Pan, Z. Chen, B. Li, and J. Song, "Biomimetic mineralized hydroxyapatite nanofiber-incorporated methacrylated gelatin hydrogel with improved mechanical and osteoinductive performances for bone regeneration," *International Journal of Nanomedicine*, vol. 17, pp. 1511-1529, 2022.

[43] W. Treesuppharat, P. Rojanapanthu, C. Siangsanoh, H. Manuspiya, and S. Ummartyotin, "Synthesis and characterization of bacterial cellulose and gelatin-based hydrogel composites for drug-delivery systems," *Biotechnology Reports*, vol. 15, pp. 84-91, 2017.

[44] C. Kaliampakou, N. Lagopati, E. A. Pavlatou, and C. A. Charitidis, "Alginate–gelatin hydrogel scaffolds; An optimization of post-printing treatment for enhanced degradation and swelling behavior," *Gels*, vol. 9, no. 11, p. 857, 2023.

[45] M. Singh, A. R. Ray, and P. Vasudevan, "Biodegradation studies on periodate oxidized cellulose," *Biomaterials,* vol. 3, no. 1, pp. 16-20, 1982.

[46] A. J. Kerin, M. R. Wisnom, and M. A. Adams, "The compressive strength of articular cartilage," *Part H: Journal of Engineering in Medicine*, vol. 212, no. 4, pp. 273-280, 1998.

[47] A. T. Estevez, T. Alberto, and Y. Abdallah, "Biomimetic approach for enhanced mechanical properties and stability of self-mineralized calcium phosphate dibasic–sodium alginate–gelatine hydrogel as bone replacement and structural building material," *Processes,* vol. 12, no. 5, pp. 944, 2024.

[48] W. Ma, M. Yang, C. Wu, S. Wang, and M. Du, "Bioinspired self-healing injectable nanocomposite hydrogels based on oxidized dextran and gelatin for growth-factor-free bone regeneration," *International Journal of Biological Macromolecules,* vol. 251, pp. 126145, 2023.

[49] M. Suhail, J.-Y. Liu, M.-C. Hung, I.-H. Chiu, M. U. Minhas, and P.-C. Wu, "Preparation, in vitro characterization, and cytotoxicity evaluation of polymeric pH-responsive hydrogels for controlled drug release," *Pharmaceutics,* vol. 14, no. 9, p. 1864, 2022.

[50] Y. Ma, X. Wang, T. Su, F. Lu, Q. Chang, and J. Gao, "Recent advances in macroporous hydrogels for cell behavior and tissue engineering," *Gels*, vol. 8, no. 10, p. 606, 2022.